Effects of low-scale landscape structures on aeolian transport processes on arable land

Nicole Siegmund[a,b,*], Roger Funk[a], Sylvia Koszinsky[a], Daniel Eduardo Buschiazzo[c,d,e], Michael Sommer[a,b]

[a] Leibniz-Centre for Agricultural Landscape Research (ZALF), Research Area 1 "Landscape Functioning", Eberswalder Str. 84, D-15374 Müncheberg, Germany
[b] Institute of Earth and Environmental Science, University of Potsdam, Karl-Liebknecht-Straße 24-25, 14476 Potsdam-Golm, Germany
[c] Faculty of Agronomy, National University of La Pampa (UNLPam), cc 300, 6300 Santa Rosa, Argentina
[d] Institute for Earth and Environmental Sciences of La Pampa (INCITAP), National Council of Scientific and Technical Research (CONICET), cc 300, 6300 Santa Rosa, Argentina
[e] National Institute for Agricultural Technology (INTA), cc 11, 6326 Anguil, Argentina

ABSTRACT

The landscape of the semiarid Pampa in central Argentina is characterized by late Pleistocene aeolian deposits, covering large plains with sporadic dune structures. Since the current land use changed from extensive livestock production within the Caldenal forest ecosystem to arable land, the wind erosion risk increased distinctly. We measured wind erosion and deposition patterns at the plot scale and investigated the spatial variability of the erosion processes. The wind-induced mass-transport was measured with 18 Modified Wilson and Cooke samplers (MWAC), installed on a 1.44 ha large field in a 20 × 40 m grid. Physical and chemical soil properties from the upper soil as well as a digital elevation model were recorded in a 20 × 20 m grid. In a 5-month measuring campaign data from seven storms with three different wind directions was obtained. Results show very heterogeneous patterns of erosion and deposition for each storm and indicate favoured erosion on windward and deposits on leeward terrain positions. Furthermore, a multiple regression model was build, explaining up to 70% of the spatial variance of erosion by just using four predictors: topsoil thickness, relative elevation, soil organic carbon content and slope direction. Our findings suggest a structure-process-structure complex where the landscape structure determines the effects of recent wind erosion processes which again slowly influence the structure, leading to a gradual increase of soil heterogeneity.

1. Introduction

The land surface of the western parts of La Pampa, Argentina has in large parts been formed by aeolian processes. Intensive winds led to a distribution of sandy and silty aeolian sediment deposits, building the parent material of the soil in the study area (Zarate and Tripaldi, 2012; Zarate, 2003). Today's landscape structure is characterized by large plains with sporadic dune structures. Because of the semiarid climatic conditions, La Pampa is in the transition zone between steppe pasture and rainfed agriculture. In the last decade the share of arable land has increased considerably, accelerated by the good prices for soy beans and corn at the world market. Under cultivation the soils of La Pampa are affected by wind erosion again. Soil losses of $0.9\,t\,ha^{-1}$ were measured on soils of loess material by Buschiazzo et al. (2007) and $1.8\,t\,ha^{-1}$ on a sandy soil, which is in the same order of magnitude like annual dust depositions in this region (0.4 to $0.8\,t\,ha^{-1}$, Buschiazzo et al., 1999; Ramsperger et al., 1998). Yet, areas of the Pampa with sandy soils show much higher erosion rates which can be seen by fresh dunes, buried fences or roads covered by sand. Extreme events are also documented by satellite images as in March 2009 and January 2010 (NASA Earth Observatory). Michelena and Irurtia (1995) estimated annual potential soil loss rates up to $178\,t\,ha^{-1}$ t in the Province La Pampa caused by wind erosion, which are in better agreement to the observed soil relocations. Besides those singular strong events, wind erosion has been recognized as a gradual soil degradation process which predominantly removes the finest and most valuable particles of a soil like silt and clay particles as well as the soil organic matter (Funk et al., 2008; Iturri et al., 2017).

While landscape structures resulting from aeolian processes are already quite well understood, the recent wind-soil interactions at the

local scale have rarely been addressed in scientific investigations so far. Erosion and deposition processes take place at the same locations and are therefore difficult to separate, because diverse factors condition erosion/deposition patterns in landscapes. Local investigations have been limited by the availability of appropriate methods for measuring aeolian sediment transport dynamics (Thomas and Wiggs, 2008; Zobeck et al., 2003). The usage of sediment catchers in large number provides a profound method for quantifying horizontal sediment transport in a high spatial resolution as shown in some studies (Sterk et al., 2012; Sterk and Raats, 1996; Uzun et al., 2016; Zobeck et al., 2003). Many studies investigated wind erosion processes on sand dunes in desert or coastal environments including topographic characteristics (Bauer et al., 2009; Hesp, 2002; Tsoar et al., 2004; Walker and Nickling, 2002). Other studies analyzed wind erosion on plane agricultural plots or only with low elevation change (Buschiazzo et al., 2007; Colazo and Buschiazzo, 2015; Uzun et al., 2016; Zhao et al., 2006) but the number of these studies still remains small (Zobeck et al., 2003; Hoffmann et al., 2008a).

The aim of this study is to investigate the effect of small local landscape structures on the spatial variability of aeolian transport processes. Special emphasis is given to the variability of transport intensity, the dynamic patterns of erosion and deposition areas and theirs relation to the topographical variability on the plot. We will investigate upon the hypothesis that wind events parallel to the topographical structure result in low aeolian transport yet high material net loss and wind events orthogonal to the topographical structure result in high transport and low net loss.

2. Materials and methods

2.1. Study area and experimental Design

The study site is located at 63.9885° W and 36.577° S (165 m asl.) in the north-eastern part of Argentina's province La Pampa (Fig. 1, left).

The site is part of the Anguil Experimental Station of the Instituto Nacional de Tecnología Agropecuarias (INTA) and has been under continuous agricultural management since the 1950s. Aeolian sediments of Holocene origin cover the entire region (INTA, 1980). In the

group of 'Chaqueño' vegetation classes the natural vegetation of the study area is classified as 'Pampeana'. This class is characterized by predominant grass steppes altering with semi-open Calden forests, *Prosopis caldenia* (Cabrera, 1976). In the study region the mean annual temperature is 16 °C and the mean annual rainfall is 550 mm, most of it during summer (between December to March) with about 80 mm per month (Aliaga et al., 2016; Casagrande and Vergara, 1996).

The experimental setup was aligned to the dominance of northern and southern winds in La Pampa. The plot was 240 m long, orientated to the main wind directions from N and S, and 60 m wide (Fig. S1). At the field site the small scale topography is hardly noticeable, but can be identified already at the larger scale by areas of lower plant cover on the aerial image of Fig. 1, taken few years ago before our measurements.

The area is dominated by Typic Ustipsamment according to the USDA classification, i.e. weakly developed A-C-profiles from sandy sediments. The mean thickness of Ah horizons is 20 cm; a petrocalcic horizon (Ck, Tosca) is partly present at around 100 cm. For the selected plot a detailed soil survey has been performed by Pürckhauer augerings in a 20×20 m raster (Fig. 1, right panel) to determine thicknesses and morphological properties of soil horizons and sediment layers. In this study "topsoil thickness" is defined as the sum of layers with dominating Ah characteristics. Further, 48 samples from the topsoil were taken for physical and chemical analysis. Soil texture was determined for a transect passing the plot and its topographical structure from north to south (Fig. 1, right panel). The location of the transect was chosen in the middle part of the plot, assuming that the variations in carbon content, nitrogen content and pH value are determined by topographical influences.

The equipment for measuring wind erosion was placed on the plot once a wind event of erosive magnitude (v > 6 m/s, de Oro and Buschiazzo, 2008) was expected to come. The setup of the erosion measurement was as follows: 24 MWAC samplers on a 20×40 m grid and two meteorological stations which measure wind velocity, wind direction, temperature and air humidity in 1 m height were installed at the northern and southern part.

The experimental setup is orientated on the predominance of northern and southern winds, shown in Fig. 2. Especially during the
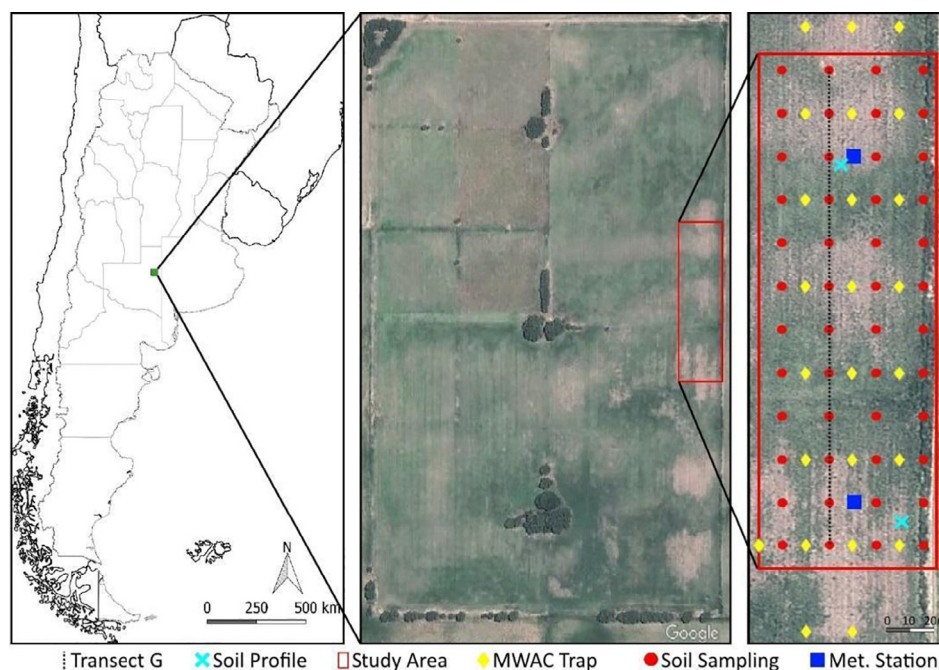

Fig. 1. Left: location of the study area in the central plateau of Argentina, South America. Center: Aerial photography of the study area. Right: experimental setup with the locations of the MWAC samplers, the soil profile pits, the transect G for texture analysis, and the meteorological stations. Source of the aerial photos: © Google Earth (2013).
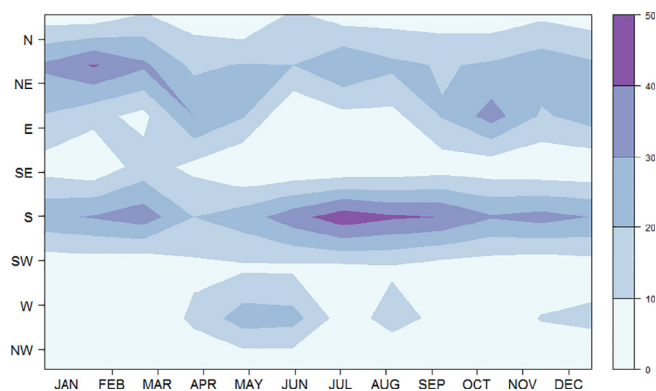
Fig. 2. Percentage of daily wind directions per month at the study site between 2012 and 2016. Included are only days with an average wind speed > 6 m/s. Data Source: http://siga2.inta.gov.ar/en/datoshistoricos/.

southern hemispheric winter to spring months these directions prevail. Against expectations, two westerly wind events have been measured during the campaign. Yet, the focus of this study is clearly on northern and southern wind events.

For this study, all shown wind measurements are averages between the two meteorological stations for the measurements 1 m above ground. Few days before the measurements the plot was prepared with a disc harrow for a bare surface. The field around the plot was under corn cultivation, but used as winter pasture for cattle. So, the plot was surrounded by an area of flat corn residues, which could be considered as non-erodible by a complete coverage of corn leaves and recumbent stems. Solely sparsely distributed annual weeds remained on the plot, covering less than 5% of the area. While the vegetation cover was insignificant for the first five erosion events, the events No. 6 and 7 had around 5% soil cover by weeds. Additionally, the plot has a fence on the eastern border, leading to a narrow vegetation covered strip.

At three spots of the middle transect, soil samples with 3 replicates have been taken for laboratory analyses to determine erodible fraction (EF_{sieved}) and the dry aggregate stability (DAS) of the soil previous to each event.

2.2. Meteorological conditions

In preparation for the measuring campaign meteorological data was analyzed to find the auspicious time of the year for wind erosion measurements and the predominant wind direction. The average annual wind-velocity is 15 km/h. The highest wind velocities arise between August and October with an average of 20–25 km/h and gusts reaching more than 60 km/h (Casagrande and Vergara, 1996). The most dominant wind direction during this period is southern and northern/northeastern, together contributing up to 80% of the windy

days (Fig. 2). Based on this analysis we decided to orientate the measuring in N-S direction.

Especially during this time of the year (southern hemispheric winter and spring) agriculturally used areas are often not covered with plants and therefore susceptible to wind erosion.

2.3. Topography

The topographic structure of the plot was measured with an optical level (Pentax AP-022) with a vertical resolution of 1 cm in a grid of 20 m. In addition, 36 points were measured outside the plot (200 m south and north, 100 m east and west) to estimate the plot's landscape position on a larger scale. The data are used to generate a digital terrain model. The measured elevation was interpolated using the ordinary point kriging interpolation algorithm provided by the ArcGIS spatial analyst toolbox. Furthermore, we used ArcGIS to calculate the topographic position index (Jenness, TPI), slope percent (Sperc) and slope direction (SD) for each of the interpolated grid points.

2.4. Chemical and physical soil analysis

Topsoil samples were air-dried and sieved through a 2 mm mesh. The pH was determined using a 0.01 M $CaCl_2$ solution with a soil-solution ratio of 1:2.5 using the Altronix/TPXIII (Schlichting et al., 1995). The total carbon (Ct) and total nitrogen content (Nt) was determined by elemental analysis (dry combustion at 1250 °C, TruSpec, LECO, Mönchengladbach) in duplicate (Din ISO 10694, 1996). Total carbon equals soil organic carbon (SOC) as all topsoils showed no carbonates. All analyses were carried out at the Central Laboratory of the ZALF in Müncheberg, Germany.

12 topsoil samples of the middle transect shown in Fig. 1 were analyzed concerning soil texture using the wet sieving and pipette method (DIN ISO 11277, 2002; Gee and Bauder, 1986). Based on these analyses the erodible fraction (EF_c) was calculated according Fryrear et al. (1998):

$$EF_c = \frac{29.09 + 0.31 \cdot Sa + 0.17 \cdot Si + 0.33 \frac{Sa}{Cl} - 2.59 \cdot OM - 0.95 \cdot CaCo_3}{100},$$

where Sa = sand content [wt.%], Si = silt content [wt.%], Sa/Cl = sand to clay ratio, OM = organic matter [wt.%] and $CaCO_3$ = calcium carbonate [wt.%].

For determining dry aggregate stability (DAS), three samples from a N-S transect at the middle of the plot were taken before each event. The three samples were sieved in a rotary sieve with 0.42 mm, 0.84 mm, 2 mm, 6.4 mm and 19.2 mm meshes (Chepil 1962). The percentage of the aggregates < 0.84 mm in diameter representing the erodible fraction (EF_{sieved}) was calculated following Colazo and Buschiazzo (2010):
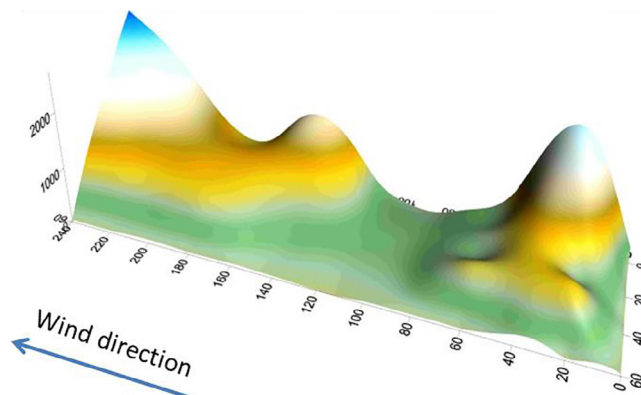

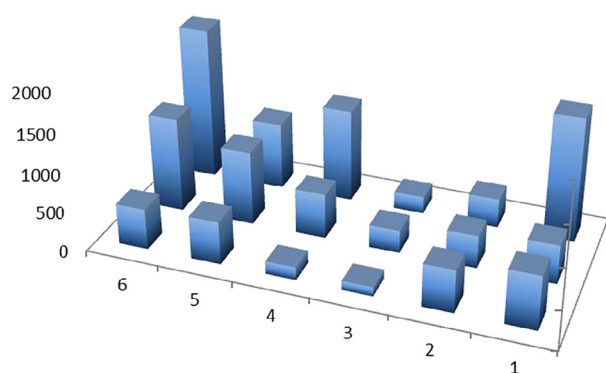**Fig. 3.** Left: calculated Q of each MWAC, right: interpolated 1 m – grid of the entire plot, example is the event at the 26.08.2016.
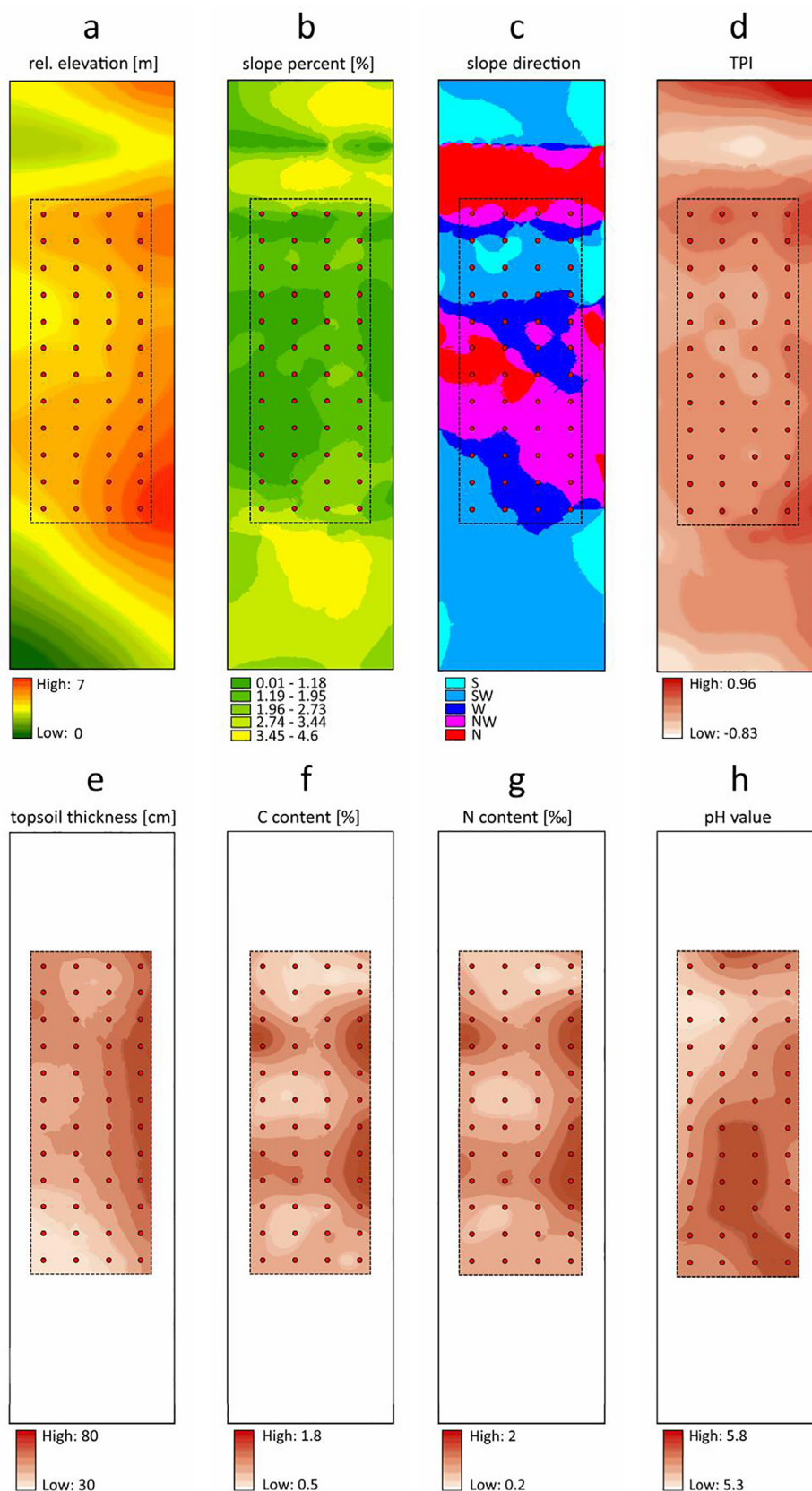
Fig. 4. Relative elevation, the slope percent, the slope direction and the topographic position index as derived from the digital elevation model (upper panels) and topsoil thickness, C and N content and the pH value as interpolated from the analysis of the topsoil samples.

Table 1
Summarized data of the seven erosion events during August 2016 to December 2016.

| Date	Event	Time	Duration	measuring Interval	WFI_6	$WFI_6\ h^{-1}$	Wind direction			Wind speed				EF_{sieved}	DAS
								mean	SD	max_{dev}	mean ms^{-1}	min ms^{-1}	max ms^{-1}	SD ms^{-1}	%	%
		hh:mm:ss	hh:mm:ss	s												
26. Aug.	1	09:52:05–15:09:35	05:17:30	5	23,049	4356	SSW	198	35	142	8	0	13	2	–	–
13. Sept.	2	09:25:00–15:39:00	06:14:00	60	119,559	19,816	SSW	199	7	17	9	6	12	1	52	74
18. Nov.	3	09:20:01–14:40:01	05:20:00	60	39,821	7471	N	8	7	18	8	3	11	1	60	71
20. Nov.	4	10:19:00–17:40:00	07:21:00	60	34,154	4647	SSE	155	14	42	7	3	10	1	54	81
04. Dec.	5	10:50:00–17:40:00	06:50:00	60	75,295	11,024	NNE	22	14	96	8	0	12	1	61	67
10. Dec.	6	10:16:00–19:10:00	08:54:00	60	99,391	11,168	WNW	303	42	84	8	1	12	1	60	68
12. Dec.	7	14:52:00–19:10:00	04:18:00	60	56,631	13,170	WSW	234	28	3	9	2	12	1	60	69
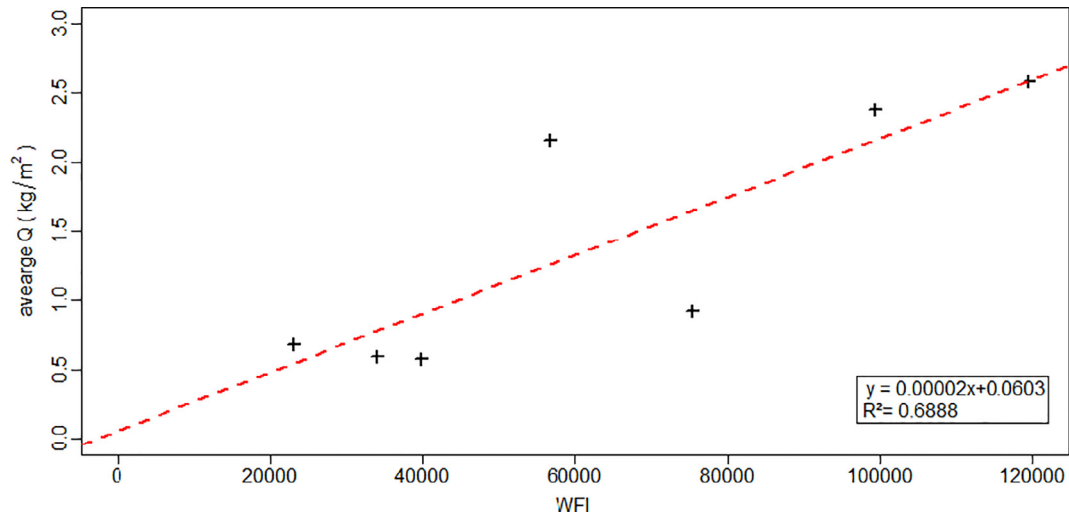
Fig. 5. Average transport rate Q on the plot in dependence on the Wind Force Integrals of each erosion event.

$$EF_{sieved} = \frac{W < 0.84}{TW} \cdot 100,$$

where EF_{sieved} = erodible fraction [%], $W < 0.84$ = weight of < 0.84 mm aggregates [g] and TW = initial weight of total sample [g].

After a second dry sieving of each aggregate size the dry aggregate stability (DAS) was calculated following Skidmore et al. (1994):

$$DAS = \left[1 - \frac{W < 0.84_2}{W > 0.84_1} \right] \cdot 100,$$

where $W < 0.84_2$ = weight of < 0.84 mm aggregates after a second sieving [g] and $W > 0.84_1$ = weight of > 0.84 mm aggregates after first sieving [g].

2.5. Measurement and calculation of soil erosion

18 Modified Wilson and Cooke (MWAC, Kuntze et al., 1990) samplers were installed on a regular 20 × 40 m grid covering the study area and additionally 6 MWAC surrounding the plot (Fig. 1, right panel). Each sampler was equipped with four bottle traps at heights of 7.5 cm, 22.5 cm, 55 cm and 110 cm. The central poles of the MWAC have wind sails in order to make sure that the devices are always aligned with wind direction. The reference height (z = 0) was set by spanning a 10 m line across the installation point of each MWAC in an acute angle to the tillage direction. Similar experimental setups have previously been used for studies like Funk et al. (2004), Mendez et al. (2011), Sterk et al. (2012) or Sterk and Raats (1996).

The traps were installed at the plot shortly before the wind events started and were collected immediately after the wind events or before announced rainfall. The trapped material of each bottle (q_z) was weighed (accuracy = 0.001 g) and used to calculate vertical profiles of

q_z by regression analysis. Two regression models were used, q_z = f(ln z) and lnq_z = f (ln z), and the one with the better R^2 was chosen to calculate the vertical integrated sediment transport rate (Q in g m^{-1}) for the heights from 0.005 m to 1.10 m (Zobeck et al. 2003) with integration steps of 0.007 m (MWAC inlet diameter), converted to 1 m width:

$$Q = \sum_{z=0.005}^{1.1} q_z \times f_{MWAC}$$

where $f_{MWAC} = \frac{7000}{38.48}$ with 7000 mm^2 resulting from the conversion to 1 m width and 38.48 mm^2 from the inlet area of the sampler ($\pi*r^2$).

To create maps of transport rates, first triangulation with linear interpolation was used to create a simple map in 1 × 1 m grid. Data was smoothed by Modified Shepard's method, which uses a quadratic polynomial fit in the neighborhood of each data point. The result is an inverse distance weighting (IDW) interpolator, but not showing the bull's-eye effect as produced by IDW. The map in the 1-m resolution was used to calculate the balance of the sediment transport at the plot by summing up the grid cells at the incoming and outgoing boundaries in relation to the wind direction of each event. As one example illustration, Fig. 3 shows the calculated Q of each MWAC at its location on the plot and the spatial interpolated Q in a 1 m – grid for the entire plot. The southern boundary was set to zero, because of the good plant residue cover at that time.

In August–September the plot was surrounded by a non-erodible pasture and soil material input from that area could be excluded. For spatial interpolation purposes the windward boundaries of the plot were set to zero. In November–December the measuring plot was influenced by possible additional inputs because of seedbed preparations on the surrounding field and additional traps were also installed outside in north, south and west.
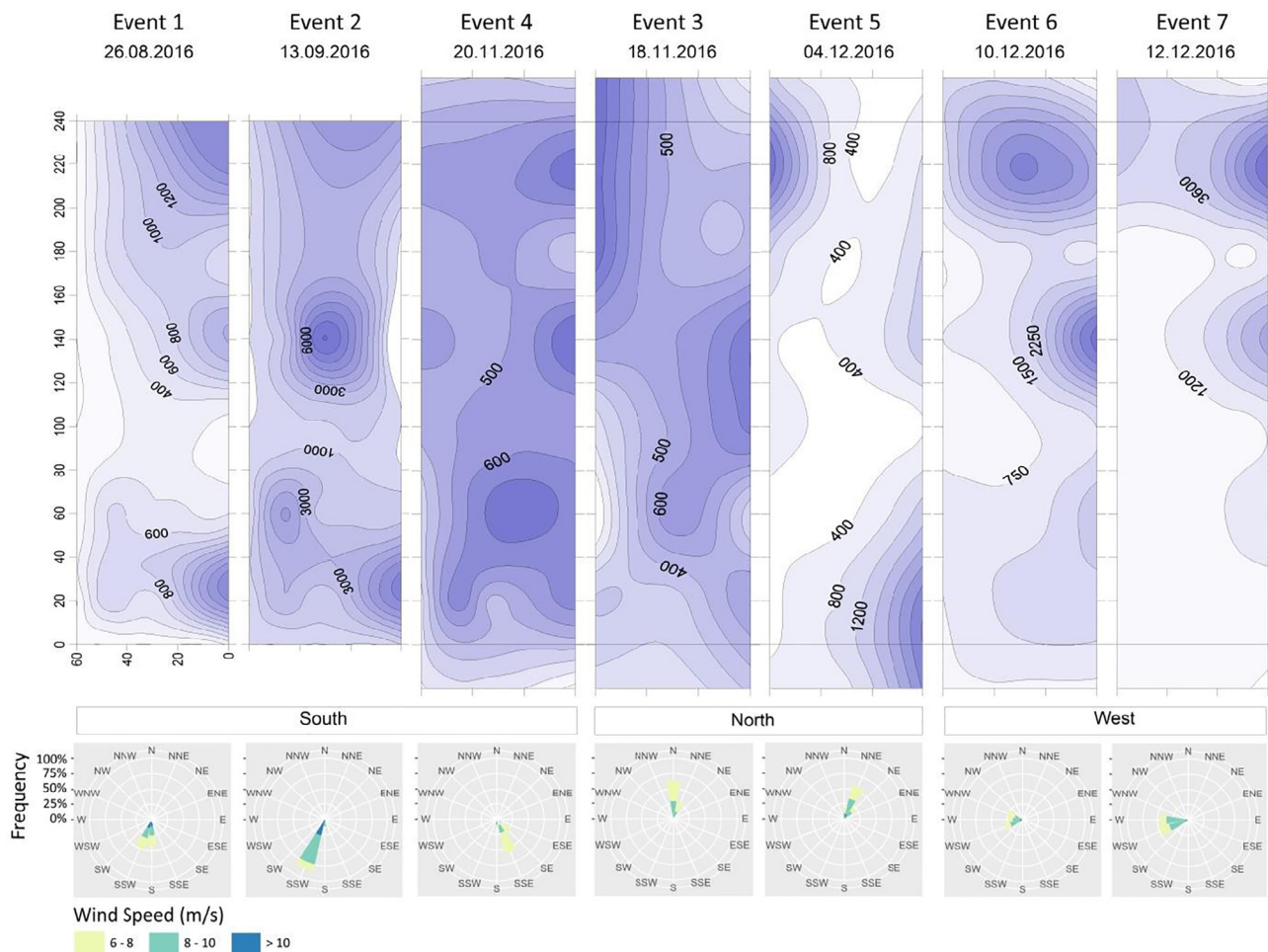
Fig. 6. Spatial distribution of the transport rates [g m^{-1}] on the plot for all measured events and frequencies of associated wind speeds and its directions.

Table 2
Accounting of net mass transport on the plot during the seven wind events. "netto" in this case is "out–in".

	Event 1 26.08.2016 SSW	Event 2 13.09.2016 SSW	Event 3 18.11.2016 N	Event 4 20.11.2016 SSE	Event 5 04.12.2016 NNE	Event 6 10.12.2016 WNW	Event 7 12.12.2016 WSW
Q$_{in}$ [kg]	0	0	45	33	79	190	258
Q$_{out}$ [kg]	351	588	29	38	113	730	895
average Q [g/m^2]	680	2570	580	600	920	2370	2150
loss netto [kg]	351	588	−16	5	34	540	637
loss netto [kg/ha]	244	408	−11	3	24	375	443

As transport rates are not necessarily correlated to local soil losses, the spatial distribution of soil loss was calculated using

$$SL_{x,y} = Q_{x,y} - Q_{x+1,y+1}$$

where $Q_{x,y}$ denotes the transport rate at position x,y of the plot and $Q_{x+1,\,y+1}$ the transport rate at next leeward raster cell. Thus, negative SL indicate erosion, positive indicate deposition in the direction of transport.

Since the events also differ by wind intensity, we calculate the wind force integral (WFI) for wind speeds at the height of 1 m according to Fryberger and Dean (1979):

$$WFI = \Sigma_t((v_t - 6)v_t^2) \cdot \Theta(v_t - 6),$$

where v_t is the wind velocity at time t and Θ describes the Heaviside function giving 0 if $v_t - 6 < 0$ and 1 if $v_t - 6 > 0$. Finally, we normalize the WFIs according to the individual duration of each event, resulting in WFI per hour. A similar procedure has already been suggested by

Hoffmann et al. (2008b).

2.6. Spatial modelling of the input parameter

For showing the spatial structure of the data and to model semi-variograms we used the geostatistical software GS+ (Gamma Design, St. Plainwell, Ml). Spherical and exponential models were fitted to the experimental semivariograms and used for ordinary kriging interpolation of relative elevation, topographic position index (TPI), topsoil thickness (TT), Ct content and Nt content (Fig. S2 and Table S1). All the data was computed untransformed since data was normally distributed. The models with the highest efficiency (R^2) and the smallest residuals were determined in order to provide the input parameters for interpolation.
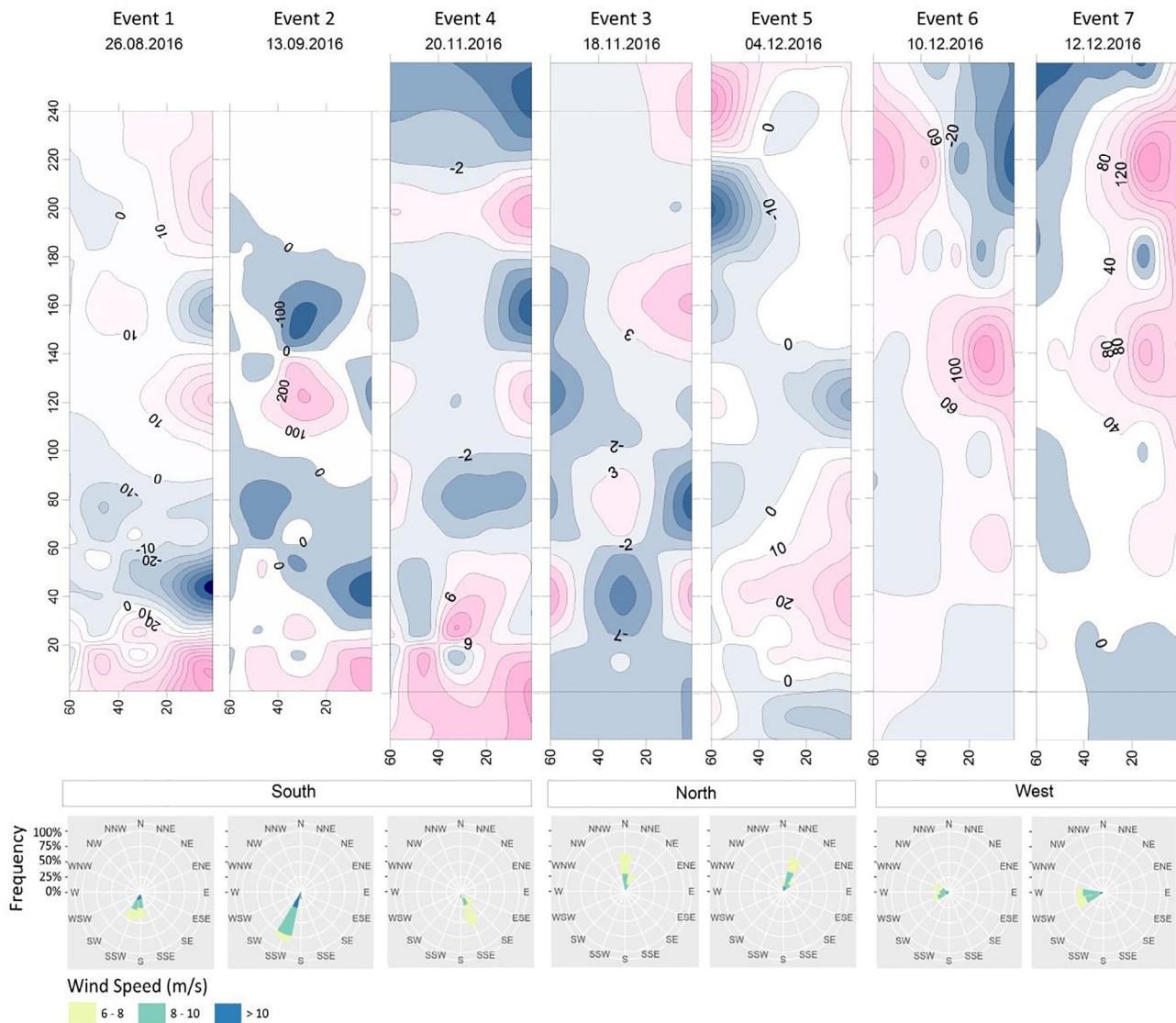
Fig. 7. Spatial distribution of erosion (red colors) and deposition (blue colors) in g m^{-1} for the seven wind events measured with MWAC sediment traps. (For interpretation of the references to colour in this figure legend, the reader is referred to the web version of this article.)

2.7. Modelling erosion by site parameter

In order to investigate the statistical relationships between pairs of soil properties as well as between pairs of erosion data and soil properties we calculate linear Pearson correlation coefficient and a standard student t-test was applied in order to proof for significance ($\alpha = 0.05$). Subsequently, a multiple linear regression model using four selected soil parameters as predictors was set up for the explanation of the measured erosion following the general equation:

$$y = a + b_1 \cdot x_1 + b_2 \cdot x_2 + \ldots + b_n \cdot x_n$$

In order to avoid multi-collinearity between the predictors (i.e. to assure statistical independency and to avoid overfitting), we only chose those parameters for the regression model, which show a correlation between each other lower than $r = 0.5$. The statistical evaluations were performed using R (R Core Team, 2014).

3. Results and discussion

3.1. Spatial patterns of terrain attributes and soil properties

Our plot shows gentle ups and downs resulting in a relative elevation difference of two meters between the highest and lowest part. The relief is very gentle with slopes less than 5 per cent (Fig. 4, b) with mainly north and south orientated slope directions (Fig. 4, c and d). The topsoil thickness is generally higher on the topographically higher parts of the plot reaching up to 63 cm (Fig. 4, e). This can also be observed for Ct and Nt contents on these elevated positions, indicating insignificance of water erosion processes (Fig. 4, f and g). The pH values show a very low variation. When comparing the soil parameters (Fig. 4, f and g) to the topographical features as rel. elevation and TPI (Fig. 4, a–d) no common patterns can be seen obviously. Contrarily, the comparatively low pH values in the northwestern part of the samples area (Fig. 4, h): exactly in this area the terrain properties also show variation in terms of low elevation (Fig. 4, a) and southern slope direction (Fig. 4, c). Nevertheless, the patterns of the soil properties exhibit high similarity amongst each other: Ct and Nt show very similar patterns.

3.2. Spatial variation of aeolian soil transport

During the southern hemispheric winter and spring season 2016 (August to December) seven erosive wind events have been measured. They differed in intensity, direction and duration but all caused measurable soil transports at the plot. Information about the dates,
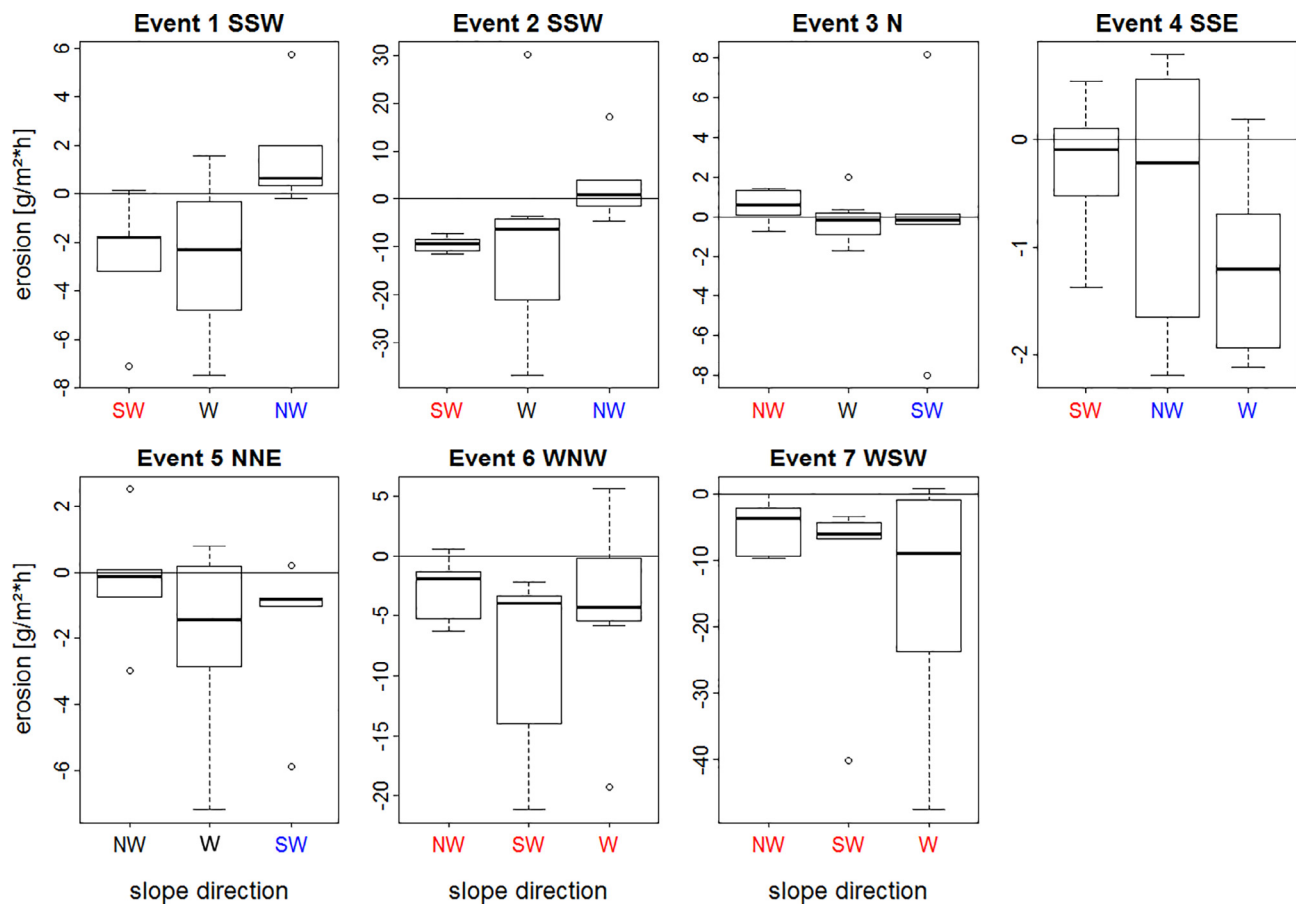
Fig. 8. Boxplots of measured erosion values of the seven wind events, classified by three slope directions: NW, SW and W. Negative values denote erosion, positive deposition. With respect to the main wind direction of the wind event, red highlighted wind directions marks windward sides, blue marks leeward sides and black text marks slopes that are parallel to the event's wind direction. (For interpretation of the references to colour in this figure legend, the reader is referred to the web version of this article.)

durations and intensities of the wind events are summarized in Table 1.

Two pedological parameters that are often discussed when investigating wind erosion are the erodible fraction and the soil aggregate stability (Kohake et al., 2010; Skidmore and Layton, 1992). Both are assumed to systematically influence the potential soil erosion during a given wind event (Colazo and Buschiazzo, 2010; Skidmore and Layton, 1992; Zobeck and Popham, 1990). In this study, we determined both parameters before every event in order to get their temporal variability.

DAS and EF_{sieved} change only slightly between the events. While DAS has a decreasing tendency on the plot, the EF_{sieved} and the erodibility on the plot increases. The percentage of erodible fractions was always smaller than 60%. Consequently, the transport rates were supply-limited. The trapped amounts and calculated transport rates were relatively low and deposits at the plot were not caused by limitations of the transport capacity of the wind.

There is a close relationship between the wind forces (WFI) and the transport rates, shown in Fig. 5 giving average transport intensity of each erosion event at the plot Despite this clear dependence between wind speed and transport rate, all events have a high spatial variability of transport rates (Fig. 6). The patterns of the spatial distribution show that the transport rates are influenced by the topographic structure, especially by windward and leeward orientated slopes. In cases where the wind direction is orthogonal to the topographic structure, increase and decrease of the transport rate follow the relief (Fig. 6, events with north–south or south-north wind directions). Wind erosion events parallel to the topographic structure are characterized by a steady increase of the transport rate with plot length, caused by the windward facing of the slopes (events 6 and 7). The very low transport rates in the south of the plot during these two west-wind events may also be a result

of coverage by weeds of around 5–10% in this area.

The calculated soil losses of this study (Table 2) agree very well with previous measurements of wind erosion in the province La Pampa. Buschiazzo et al. (2007) found losses between 4 and 900 kg ha^{-1} and accumulations between 3 and 580 kg ha^{-1} on typical soil types of this region. Ramsperger et al. (1998) reported deposits between 114 and 365 kg ha^{-1} month^{-1}, mainly of the dust fractions. The erosion values found in this study ranged between 5 and 500 kg ha^{-1} per event which fit well to the previously measured erosion rates for this region of Argentina. As already stated by Sterk and Stein (1997) and Visser et al. (2004), the simple comparison of incoming and outgoing fluxes can result in incorrect estimates of soil transport at a field, it is more useful to distinguish erosion and deposition areas in the plot. An important consequence results, if horizontal fluxes are related to vertical fluxes (dust emissions).

3.3. Spatial patterns of erosion and deposition

Converting the transport rates into spatial patterns of erosion and deposition results in the maps shown in Fig. 7. Areas of erosion and deposition alternate in small patterns and are located in immediate vicinity, especially for the North and South events. Events from the same direction show similar patterns.

To indicate the influence of the slope direction on spatial patterns, the calculated values of erosion or deposition from the maps in Fig. 7 are illustrated with boxplots, where all MWAC positioned within the same category of slope direction contribute to one boxplot (Fig. 8). Windward and leeward positions show clearly differing distribution parameters, where especially strong events show distinct differences
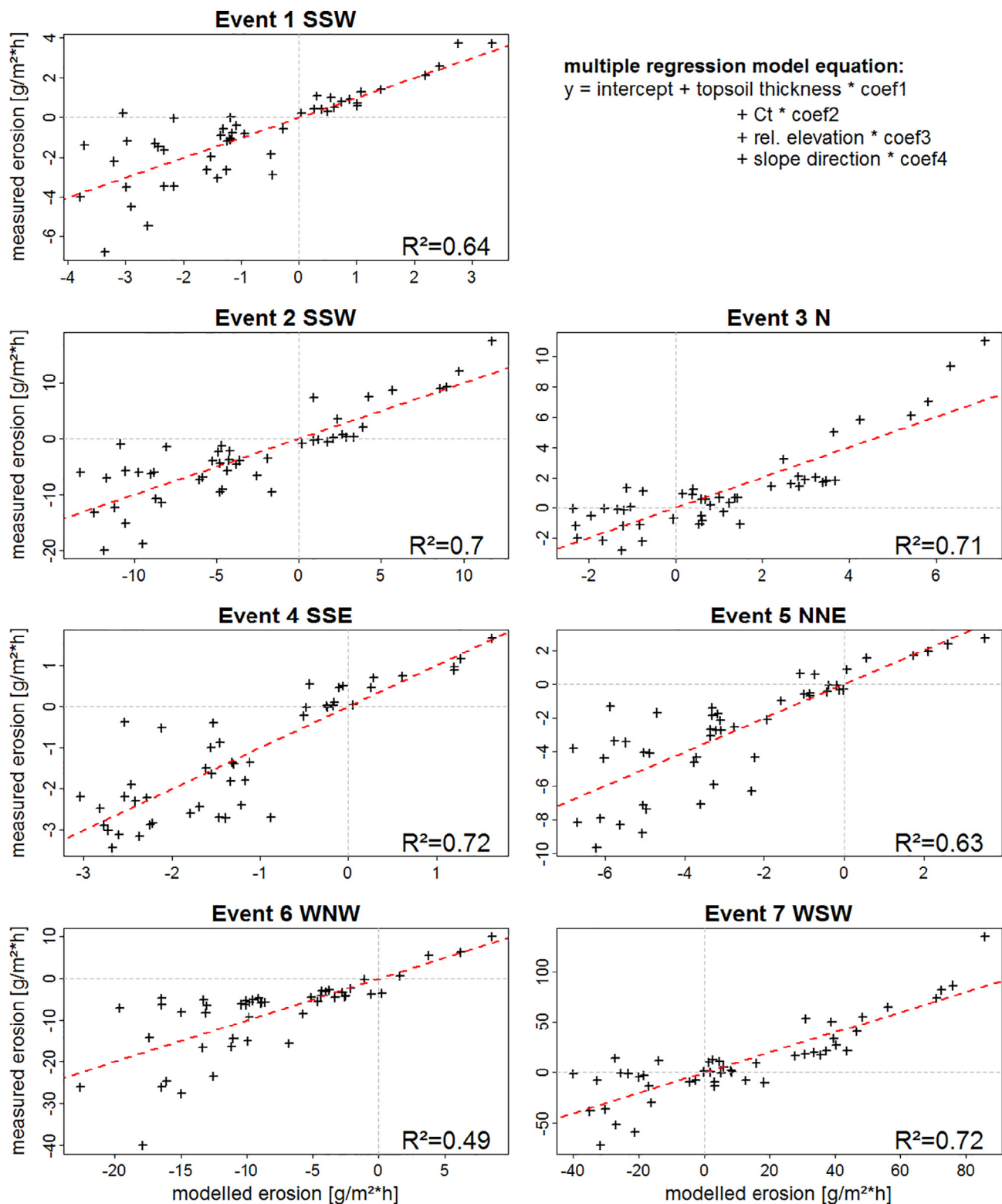
multiple regression model equation:
y = intercept + topsoil thickness * coef1
+ Ct * coef2
+ rel. elevation * coef3
+ slope direction * coef4

Fig. 9. Measured versus modelled erosion for all seven wind events and the related explained variance (R^2) using a multiple linear regression model with topsoil thickness, Ct, relative elevation and slope direction as predictors. The red lines mark x = y. (For interpretation of the references to colour in this figure legend, the reader is referred to the web version of this article.)

between erosion and deposition areas. For opposite wind directions (N–S, S–N) windward and leeward positions change, i.e. these positions alter between deposition and erosion areas.

A similar analysis was performed for the impact of different TPI positions on erosion (Fig. S3), but erosion and deposition were not linked with this topographical characteristics. The TPI information

therefore is excluded from the following analyses.

The strong spatial variability of wind erosion at the plot clearly underlines the intensive affection of erosion processes by even only small topographic changes. Uzun et al. (2016), Visser et al. (2004) and Sterk et al. (2004) also presented maps of spatial erosion distributions for study areas with even lower topographical variability, but also

Table 3
Intercept and the coefficients of the seven multiple regression models for the erosion resulting from the seven wind events.

event	intercept	coef1 TT	coef2 Ct	coef3 Ele	coef4 SD
1	− 221.47	− 0.05	1.18	2.23	0.06
2	− 810.34	− 0.16	5.54	8.15	0.15
3	− 340.83	− 0.04	1.78	3.45	0.10
4	− 158.90	− 0.03	1.26	1.59	− 0.03
5	− 338.82	− 0.06	1.82	3.40	− 0.18
6	− 868.02	− 0.21	1.51	8.74	− 0.23
7	− 4111.69	− 0.79	29.30	41.60	0.37

indicated such heterogenic patterns. Similar to our findings, Uzun et al. (2016) also revealed that the heterogeneity of erosion and deposition is increasing with stronger wind events.

A critical issue on studies like this, dealing with sediment catchers for soil erosion measurements, is the question of uncertainty. Uncertainty can come into effect on both, the measurement and the data processing side: even small errors/uncertainties in the measurements can, as a result of the integrating data processing, propagate and finally accumulate – bearing a high potential for uncertainty in the results. Tidjani et al. (2011) comprehensively investigated on the uncertainties for soil erosion measurements and calculations like in our analysis. Following Tidjani et al. (2011), the largest part of uncertainty comes due to weighing uncertainty, because this effect accumulates through the calculations. We used a Precisa 125A with a precision of 0.001 g where the weighing was conducted under laboratory conditions. The uncertainty of measuring with MWAC samplers strongly depends on the trapping efficiency. The MWAC traps used in this study have inlet diameters of 7 mm, which prove to come with very high trapping efficiency (~ 90%) in comparison to other models.

3.4. Statistical modelling of erosion and deposition

Before constructing a multiple regression model using topographic and soil parameters as predictors for wind erosion/deposition in the spatial domain, we conducted a comprehensive correlation analyses for all possible pairs of topographic soil parameters (see Table S3, where only significant correlation coefficients are given. Significance was tested using a standard Student T-test with alpha = 0.05). This allows for the construction of a multiple linear regression model, on the one hand including all parameters that are well correlated with erosion ("forward-selection" approach) and on the other hand excluding multicollinearity and therefore over-fitting as far as possible. Based on this correlation matrix, the following parameters were chosen for the construction of the regression models (Fig. 9): topsoil thickness (TT [cm]), Ct [‰], relative elevation (Ele [m]) and slope direction (SD [no unit]), resulting in the general regression equation:

$$y = intercept + top\ soil\ thickness \cdot coef_1 + Ct \cdot coef_2 + rel.\ elevation \cdot coef_3$$
$$+ slope\ direction \cdot coef_4$$

Although the slope direction (SD) does not show significant correlations with erosion in Table S3 (a), this parameter was included into the model because in Fig. 8 the clear influence of classified slope directions at least for some of the events could already be shown. In order to transform slope direction (SD) into a variable giving information about wind- and leewards directed slopes, we apply:

$$SD^n = cos(SD - \overline{wdir_n})$$

,where $\overline{wdir_n}$ is the mean wind direction of the specific event n. The new variable SD^n is 1 when the slope direction is fully windward to the average wind direction of event n and − 1 when the slope direction is fully leeward to the average wind direction of event n. For simplicity, yet, SD^n is consistently abbreviated by SD in the remaining.

The coefficients of the predictors (Table 3) vary for each individual event.

The explained variance (R^2) of the modelled erosion/deposition ranges from 50% to 75% where most of the models exhibit an $R^2 > 0.7$. Except of the events 3 and 7, the model almost never mismatches positive and negative erosion. A skewness of the distribution of residuals cannot be seen which makes the linear modelling approach seem reasonable for the given data set.

Except for slope direction, the coefficients are consistently either positive or negative for all events which means, that greater topsoil thickness is linked to higher erosion (negative coefficient) and a higher Ct content is always linked to higher deposits (positive coefficient) in every wind event.

Investigations of Hong et al. (2014) or Zobeck et al. (2013) presented similar studies, showing models with explained variances of around 0.61 and 0.94 using the topsoil water content, soil fractions, wind erodible fraction (EF) and organic matter as predictors. The fact that the models perform well for all seven wind events underlines the importance of topographical changes on wind erosion/deposition processes and shall sensitize for designs of field experiments.

The analysis of the soil texture along the transect shown in Fig. 1 revealed only marginal variations of soil texture within the plot. Therefore no further statistical evaluations with texture have been conducted.

4. Conclusions

This study shows that the topographical structures in the study area influence the variability of recent aeolian processes, whereas pedology has lower importance caused by the homogeneous soil parameter in the investigation area. Based on investigations of the spatial distribution of the sediment fluxes, maps of erosion/deposition patterns were derived. Depending on the wind direction of each erosion event, distinct patterns of erosion/deposition could be identified. Soil material is preferentially eroded from the windward slopes and deposited on the leeward flanks in the immediate. This is a direct impact on the structure itself and slowly changes the terrain and soil properties of the plot. Over long periods these changes can evolve, because of the predominance of only two wind directions in La Pampa in the periods with bare soils, and the removal of SOM and nutrients with the dust fractions. Our study verifies the strong spatial variability of wind erosion processes caused by even small changes of the controlling factors. These spatial variabilities lead to a gradual change of the soil heterogeneity and should be considered in experimental setups for field measurements.

Appendix A. Supplementary data

Supplementary data associated with this article can be found, in the online version, at http://dx.doi.org/10.1016/j.aeolia.2018.03.003.

References

Aliaga, V.S., Ferrelli, F., Alberdi-Algañaraz, E.D., Bohn, V.Y., Piccolo, M.C., 2016. Distribución y variabilidad de la precipitación en la región Pampeana, Argentina. Cuader. Investig. Geogr. 42 (1), 261–280.
Bauer, B., Davidson-Arnott, R., Hesp, P., Namikas, L., Ollerhead, J., Walker, I., 2009. Aeolian sediment transport on a beach: surface moisture, wind fetch and mean transport. Geomorphology 105, 106–116.
Buschiazzo, D.E., Zobeck, T.M., Abascal, S.A., 2007. Wind erosion quantity and quality of an Entic Haplustoll of the semi-arid pampas of Argentina. J. Arid Environ. 69, 29–39.

Buschiazzo, D.E., Zobeck, T.M., Aimar, S., 1999. Wind erosion in loess soils of the semiarid Argentinian pampas. Soil Sci. 164 (2), 133–138.

Cabrera, A.L., 1976. Regiones fitogeográficas argentinas. In: Kugler, W.F. (Ed.), Enciclopedia Argentina de Agricultura y Jardineria II. ACME, Buenos Aires, pp. 1–85.

Casagrande, G., Vergara, G., 1996. Características climática de la region. In: Buschiazzo, D.E., Panigatti, J.L., Babinec, F.J. (Eds.), Labranzas en la región semiárida Argentina. INTA, pp. 11–19.

Chepil, W.S., 1962. A compact rotary sieve and the importance of dry sieving in physical soil analysis. Soil Sci. Soc. Am. Proc. 26, 4–6.

Colazo, J.C., Buschiazzo, D.E., 2010. Soil dry aggregate stability and wind erodible fraction in a semiarid environment of Argentina. Geoderma 159, 228–236.

Colazo, J.C., Buschiazzo, D.E., 2015. The impact of agriculture on soil texture due to wind erosion. Land Degrad. Dev. 26, 62–70.

De Oro, L., Buschiazzo, D.E., 2008. Threshold wind velocity as an index of soil susceptibility to wind erosion under variable climatic conditions. Land Degrad. Dev. 20, 14–21.

DIN ISO 10694, 1996. Soil Quality – Determination of Organic and Total Carbon After Dry Combustion (Elementary Analysis) (ISO 10694:1995). Beuth Verlag, Berlin.

DIN ISO 11277, 2002. Soil Quality – Determination of Particle Size Distribution in Mineral Soil Material – Method by Sieving and Sedimentation (ISO 11277:2009). Beuth Verlag, Berlin.

Fryberger, S.G., Dean, G., 1979. Dune Forms and Wind Regime. in: McKee, E.D. (Ed.), A Study of Global Sand.

Fryrear, D.W., Saleh, A., Bilbro, H.M., Schomberg, J.E., Zobeck, T.M., 1998. Revised Wind Erosion Equation (RWEQ). Technical Bulletin 1. Southern Plains Area Cropping Systems Research Laboratory, Wind Erosion & Water Conservation Research Unit, USDA-ARS.

Funk, R., Reuter, H.I., Hoffmann, C., Engel, W., Otti, D., 2008. Effect of moisture on fine dust emission from tillage operations on agricultural soils. Earth Surf. Proc. Land. 33 (12), 1851–1863.

Funk, R., Skidmore, E.L., Hagen, L.J., 2004. Comparison of wind erosion measurements in Germany with simulated soil losses by WEPS. Environ. Modell. Software 19, 177–183.

Gee, G.W., Bauder, J.W., 1986. Particle size analysis. In: Klute, A. (Ed.), Methods of Soil Analysis, Part 1: Physical and Mineralogical Methods. American Society of Agronomy, Soil Science Society of America, pp. 383–411.

Hesp, P., 2002. Foredunes and blowouts: initiation, geomorphology and dynamics. Geomorphology 48, 245–268.

Hoffmann, C., Funk, R., Wieland, R., Li, Y., Sommer, M., 2008a. Effects of grazing and topography on dust flux and deposition in the Xilingele grassland, Inner Mongolia. J. Arid Environ. 72, 792–807.

Hoffmann, C., Funk, R., Li, Y., Sommer, M., 2008b. Effect of grazing on wind driven carbon and nitrogen ratios in the grasslands of Inner Mongolia. Catena 75 (2), 182–190.

Hong, S.-W., Lee, I.-B., Seo, I.-H., Kwon, K.-S., Kim, T.-W., Son, Y.-H., Kim, M., 2014. Measurement and prediction of soil erosion in dry field using portable wind erosion tunnel. Biosyst. Eng. 118, 68–82.

INTA, 1980. Caracterización general de la provincia, in: Inventario integrado de los recursos naturales de la provincia de La Pampa, Buenos Aires, pp. 36–38.

Iturri, L.A., Funk, R., Leue, M., Sommer, M., Buschiazzo, D.E., 2017. Wind sorting affects differently the organo-mineral composition of saltating an particulate materials in contrasting texture agricultural soils. Aeolian Res. 28, 39–49.

Kohake, D.J., Hagen, L.J., Skidmore, E.L., 2010. Wind erodibility of Organic Soils. Soil Sci. Soc. Am. J. 74 (1), 250–257.

Kuntze, H., Beinhauer, R., Tetzlaff, G., 1990. Quantification of Soil Erosion by Wind: I. Final Report of the BMFT Project. Project No. 0339058 A, B, C. Institute of Meteorology and Climatology, University of Hannover, Germany.

Mendez, M.J., Funk, R., Buschiazzo, D.E., 2011. Field wind erosion measurements with big spring number eight (BSNE) and modified Wilson and Cook (MWAC) samplers. Geomorphology 129 (1–2), 43–48.

Michelena, R.O., Irurtia, C.B., 1995. Suspectibility of soil to wind erosion in La Pampa province, Argentina. Arid Soil Res. Rehabil. 9, 227–234.

R Core Team, 2014. R: A Language and Environment for Statistical Computation. R Foundation for Statistical Computing, Vienna, Austria URL: www.R-project.org.

Ramsperger, B., Peinemann, N., Stahr, K., 1998. Deposition rates and characteristics of aeolian dust in the semi-arid and sub-humid regions of the Argentinean Pampa. J. Arid Environ. 39, 467–476.

Schlichting, E., Blume, H.P., Stahr, K., 1995. Bodenkundliches Praktikum. Hamburg-Berlin. Seas, US Government Printing Office, Washington D.C., pp. 137–169.

Skidmore, E.L., Hagen, L.J., Armburst, D.V., Durar, A.A., Fryrear, D.W., Potter, K.N., Wagner, L.E., Zobeck, T.M., 1994. Methods for investigating basic processes and conditions affecting wind erosion. In: Lal, R. (Ed.), Soil Erosion Research Methods. Soil & W. Cons. Soc, Ankeny, USA, pp. 259–330.

Skidmore, E.L., Layton, J.B., 1992. Dry soil aggregate stability as influenced by selected soil properties. Soil Sci. Soc. Am. J. 56 (2), 557–561.

Sterk, G., Raats, P.A.C., 1996. Comparison of models describing the vertical distribution of wind-eroded sediment. Soil Sci. Soc. Am. J. 60 (6), 1914–1919.

Sterk, G., Parigiani, J., Cittadini, E., Peters, P., Scholberg, J., Peri, P., 2012. Aeolian sediment mass fluxes on a sandy soil in Central Patagonia. Catena 95, 112–123.

Sterk, G., Stein, A., 1997. Mapping wind-blown mass transport by modeling variability in space and time. Soil Sci. Soc. Am. J. 61 (1), 232–239.

Sterk, G., Stein, A., Stroosnijder, L., 2004. Wind effects on spatial variability in pearl millet yields in the Sahel. Soil Tillage Res. 76, 25–37.

Thomas, D.S.G., Wiggs, G.F.S., 2008. Aeolian system responses to global change: challenges of scale, process and temporal integration. Earth Surf. Proc. Land. 33 (9), 1396–1418.

Tidjani, A.D., Bielders, C.L., Rosillon, D., Ambouda, K.J.M., 2011. Uncertainties in plot-scale mass balance measurements using aeolian sediment traps. Soil Water Manage. Conserv. 75 (2), 708–718.

Tsoar, H., Blumberg, D., Stoler, Y., 2004. Elongation and migration of sand dunes. Geomorphology 57, 293–302.

Uzun, O., Kaplan, S., Basaran, M., Saygin, S., Youssef, F., Nouri, A., Ozcan, A., Erpul, G., 2016. Spatial distribution of wind-driven sediment transport rate in a fallow plot in Central Anatolia, Turkey. Arid Land Res. Manage. 31 (2), 1–15.

Visser, S., Sterk, G., Snepvangers, J., 2004. Spatial variation in wind-blown sediment transport in geomorphic units in northern Burkina Faso using geostatistical mapping. Geoderma 120, 95–107.

Walker, I., Nickling, W., 2002. Dynamics of secondary airflow and sediment transport over and in the lee of traverse dunes. Prog. Phys. Geogr. 26 (1), 47–75.

Zarate, M.A., 2003. Loess of southern South America. Quat. Sci. Rev. 22 (18–19), 1987–2006.

Zarate, M.A., Tripaldi, A., 2012. The aeolian system of central Argentina. Aeolian Res. 3, 401–417.

Zhao, H.L., Yi, X.Y., Zhou, R.L., Zhao, X.Y., Zhang, T.H., Drake, S., 2006. Wind erosion and sand accumulation effects on soil properties in Horqin Sandy Farmland, Inner Mongolia. Catena 65 (1), 71–79.

Zobeck, T.M., Popham, T.W., 1990. Dry aggregate size distribution of sandy soils as influenced by tillage and precipitation. Soil Sci. Soc. Am. J. 54 (1), 198–204.

Zobeck, T.M., Sterk, G., Funk, R., Rajot, J.L., Stout, J., van Pelt, R.S., 2003. Measurement and data analysis methods for field-scale wind erosion studies and model validation. Earth Surf. Proc. Land. 28, 1163–1188.

Zobeck, T.M., Baddock, M., Van Pelt, R.S., Tatarko, J., Acosta-Martinez, V., 2013. Soil property effects on wind erosion of organic soils. Aeolian Res. 10, 43–51.